Flux growth and liquid-phase epitaxy of Mn⁶⁺-doped barium sulfate

D. Ehrentraut*, **Y.E. Romanyuk and M. Pollnau**

Advanced Photonics Laboratory, Institute for Imaging and Applied Optics, Swiss Federal Institute of Technology, CH-1015 Lausanne, Switzerland

*Institute of Multidisciplinary Research for Advanced Materials, Fukuda Lab., Tohoku University, Katahira 2-1-1, Aoba-ku, Sendai 980-8577, Japan

We investigated the conditions for the growth of Mn⁶⁺-doped from the ternary eutectic NaCl-KCl-CsCl solvent at temperatures of 480-600°C. The doping complex ion MnO_4^{2-} can easily substitute the SO_4^{2-} complex ion in $BaSO_4$ with its orthorhombic space group *Pnma*. The growth of Mn⁶⁺-doped $BaSO_4$ was performed using liquid-phase epitaxy by applying an advanced growth strategy. High-quality layers were grown according to the step-flow mode with step heights of maximum 1.5 unit cells and step widths of 200 nm. The defect density was reduced to 1×10^3 and 7×10^4 etch pits cm^{-2} for (011) and (001), respectively. The growth velocity was one and two unit cells s^{-1} for ⟨001⟩ and ⟨011⟩, respectively.

Key words: Barium sulfate, Manganese doping, Stability of manganese, Flux growth, Liquid-phase epitaxy.

Introduction

The transition-metal ion Mn⁶⁺ is a promising activator ion for potential applications as tunable and short-pulse lasers because of its broadband luminescence in the spectral region 850-1600 nm. Its simple $3d^1$ electron configuration excludes undesirable exited-state absorption into higher excited 3d levels. However, hexavalent manganese can be stabilized only in the tetrahedral oxo-coordination and easily reduces to Mn^{5+}/Mn^{4+} at temperatures above 600°C. Unseeded flux growth [1] and liquid-phase epitaxy (LPE) [2] of Mn⁶⁺-doped have been reported. The incorporation of Mn⁶⁺ into different host materials with tetrahedral oxo-coordination has been investigated in detail [3]. Not only the ion radii and coordination within the XO_4^{2-} complex but also the coordination sphere of the XO_4^{2-} complex plays a significant role for the incorporation of Mn⁶⁺ [3]. Moreover, reduction of the Mn⁶⁺ ion cannot be avoided even at low temperatures and in the presence of stabilizing additives such as K_2CO_3 and NaOH. As a consequence, the concentration of Mn⁶⁺ incorporated into the grown layers decreases with growth time [3].

LPE is a powerful method allowing the growth of high-quality layers of materials, which possess either a phase transition or lack a congruent melting point, as is both the case for $BaSO_4$. We employed LPE to grow Mn⁶⁺-doped $BaSO_4$ layers with high crystalline quality by applying an improved growth strategy [2, 4]. The results from LPE as well as from the unseeded flux growth are discussed here in greater detail.

Experimental

Alkaline and earth-alkaline chlorides were used to dissolve the solute $BaSO_4$. The experiments for the unseeded flux growth, named flux growth in the further discussion, and the LPE were prepared in the way described in [3, 5]. While different solvents were employed for the flux growth of $BaSO_4$, the eutectic NaCl-KCl-CsCl was the sole solvent used for the LPE of $BaSO_4$. The experiments were carried out under ambient atmosphere and pressure in a resistance heated furnace at growth temperatures T_G between 480-600°C and 490-570°C, at cooling rates of 1-2 and 0.67 K h^{-1}, for the flux growth and LPE, respectively. For the latter, a seed crystal was situated in the center of the upper half in the solution volume and a rotation rate of 20 rpm was applied.

The grown crystalline $BaSO_4$ is water-insoluble and can be liberated easily from adherent solvent after the experiment by rinsing with distilled water. The crystals were checked for phase purity by X-ray powder diffraction (XRD) using a diffractometer (X'PERT MPD, PANalytical) in Bragg-Brentano geometry. Cu K_α radiation and silicon as the internal standard were used. The raw data from the measurements were refined by applying the Rietveld-refinement method [6]. The full-width-at-half-maximum (FWHM) was determined. Optical characterization was carried out by means of both transmission and Nomarski differential interference microscopy (N-DIM), Leica AG. Atomic-force microscopy (AFM), Explorer model from Topometrix, in contact

*Corresponding author:
 Tel : +81-22-217-5167
 Fax: +81-22-217-5102
 E-mail: dirk@tagen.tohoku.ac.jp

mode served to investigate the surface morphology of our layers. The etch-pit density (epd) was estimated by counting the etch pits obtained through slightly dissolving the specimen. The manganese concentration was estimated with electron probe microanalysis (EPMA) using a Cameca SX50 model with an acceleration voltage of 20 kV.

Crystal Growth of BaSO₄

Flux Growth of undoped BaSO₄

Well-facetted crystals up to 2 cm in $\langle 100 \rangle$ could be grown. The habit consisted of $\{011\}$, $\{101\}$, and $\{210\}$
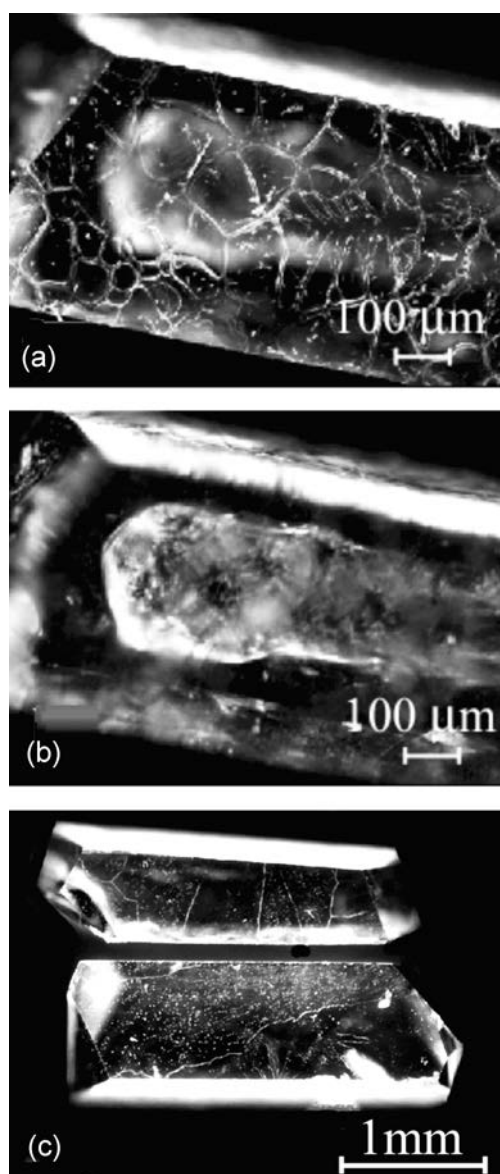
Fig. 1. (a) Details of the (011) surface of a LiCl flux-grown . The surface is dominated by its dendritic morphology. (b) Focussing inside the same crystal shows a large inclusion of mother solution. The trapped inclusion body develops the typical baryte habit when the supersaturation of the solution drops to a level small enough to allow for stabilized growth. (c) Microphotograph of flux-grown BaSO₄ crystals without inclusion of mother solution.

faces whereas well-developed $\{001\}$ faces appeared rather rarely. The surface morphology of the faces was characterized by dendrites of up to several 100 μm in length, see Fig. 1a. Dendritic crystal growth, which is a form of instable growth in the fastest growing directions, can appear at highly supersaturated regions in the flux. The supersaturation which occurs owing to the large cooling rate in flux-growth experiments decreases by the fast growth of dendrites. In addition, dendrites at the surface occur during the phase transition of the solution from liquid to solid. This process does not occur simultaneously in all regions of the flux. Consequently, nucleation is produced in the still liquid parts of the solution and dendrites start to grow. The entire process is stopped after complete solidification of the flux.

Another common feature of flux-grown crystals is the inclusion of mother solution, see Fig. 1b. It appears immediately after the homogeneous nucleation, which requires much higher supersaturation than the subsequent growth [7]. The growth is dendritic until the initial high supersaturation is consumed. Afterwards, the growth is driven by the programmed temperature-ramp-controlled supersaturation. The trapped mother solution is a source for dislocations [8]. The layer which seals the inclusion may be deformed due to pressure decrease inside the inclusion volume as a result of solute crystallization in the wrapped solution. The sealing layer bends and, thus, a misfit arises at the interface and dislocations are induced. The growth of crystals with low content of visible inclusions is possible by the unseeded flux method using the eutectic NaCl-KCl-CsCl. Figure 1c shows such a BaSO₄ crystal with a length of about 3 mm in the c-direction.

The following growth strategy [2, 4] was applied in order to obtain high-quality layers. Firstly, we grew undoped bulk samples of by the flux method. Secondly, an undoped layer was grown by LPE, and finally, the Mn^{6+}-doped layer was grown on top of the undoped layer.

Liquid-Phase Epitaxy of BaS₁₋ₓMnₓO₄

The addition of K_2MnO_4 into the solution leads to MnO_2 precipitation. These precipitates cause the heterogeneous nucleation and growth of $BaS_{1-x}Mn_xO_4$ solute crystals at the bottom of the growth container due to the lowered Gibbs energy of nucleation. This process occurred already before dipping the substrate into the liquid solution and continued during the epitaxial growth process on the substrate. As a result, each BaSO₄ crystal from the bottom of the crucible contains dark inclusions of sizes typically between 1 and 50 μm, which are localized mainly at the center of each crystal. The number of incorporated MnO_2 precipitates as well as their sizes decrease with increasing distance from the crystal nucleus and the outer
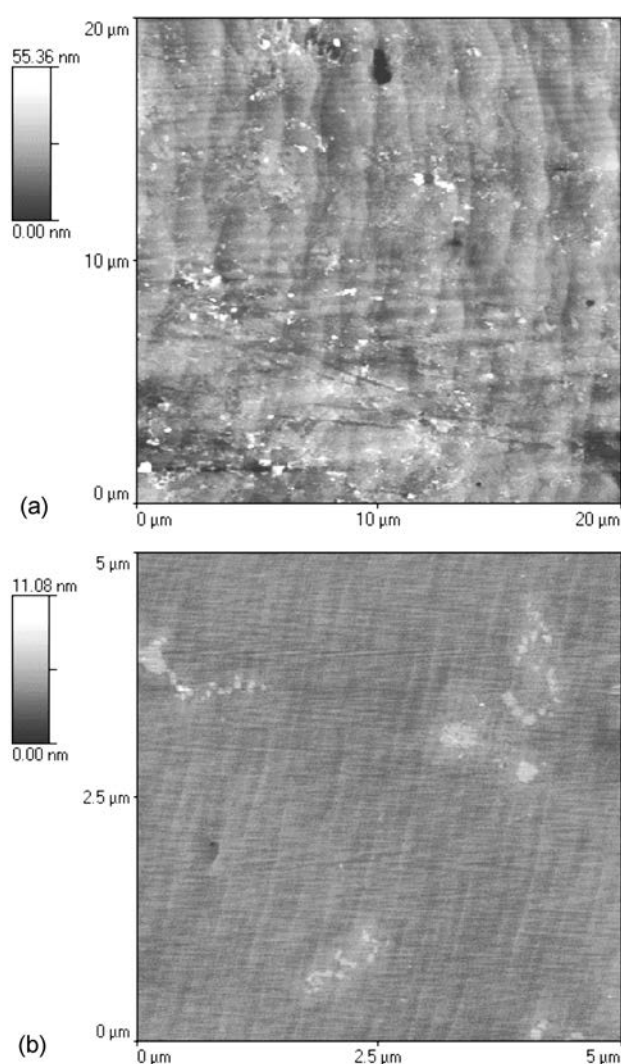
Fig. 2. AFM images (contact mode in air) of (001) surfaces: (a) Growth according to the step-bunching mechanism with step heights between 7 and 14 unit cells. (b) Growth according to the step-flow mechanisn with step heights of maximum 1.5 unit cells.

regions are typically free of MnO_2 precipitates. Furthermore, the temperature at the bottom of the container was 1°C lower than in the region where the substrate was placed. This may support the growth of crystals at the container bottom. Generally, the competing growth of additional $BaS_{1-x}Mn_xO_4$ crystals causes reduced supersaturation of the $BaSO_4$ solute in a shorter time span. The best LPE layers have been grown from saturated solutions achieved by the above-mentioned process. In contrast, nucleation of $BaSO_4$ at the bottom of the growth container was found to be negligible for the LPE growth of undoped $BaSO_4$ on flux-grown $BaSO_4$.

Surface flatness is closely connected with supersaturation of the solution. Reduced supersaturation results in a change of the growth mechanism as demonstrated by the AFM measurements in Figs. 2a-b. The growth range was between 550 and 510°C and the

cooling rate remained constant at 0.67 K h^{-1}. Growth of $BaS_{0.997}Mn_{0.003}O_4$ under conditions rather far away from the thermodynamic equilibrium is imaged in Fig. 2a. The concentrations of $BaSO_4$ and K_2MnO_4 were $c_{BaSO_4} = 4$ wt% and $c_{K_2MnO_4} = 1.2 \times 10^{-2}$ wt% with respect to the total weight of the solution. The growth process of the (001) surface followed the step-bunching mechanism. The step width measured from one top to the next is up to 2 μm. The height between consecutive steps ranges from 50 to 100 Å, or 7 to 14 unit cells in $\langle 001 \rangle$, respectively. The front of the bunched steps consists of convex parts, which suggests an effect due to impurities [8]. Adsorbed impurities on the surface stop the layer growth at the contact site. The layer continues to grow around the impurity and finally, the impurity is trapped into the layer. The impurity may consist of precipitated MnO_2 that appears in the volume of the solution. Numberless sub-micrometre sized solution precipitates are visible at the surface. Again, this is a suggestion that the problem of reduced crystal quality is due to MnO_2 precipitates trapped in the growing $BaS_{1-x}Mn_xO_4$ layer.

By contrast, Fig. 2b shows a high-quality (001) surface of a $BaS_{0.997}Mn_{0.003}O_4$ layer. The concentrations of $BaSO_4$ and K_2SO_4 were $c_{BaSO_4} = 3.75$ wt% and $c_{K_2MnO_4} = 1.2 \times 10^{-2}$ wt% with respect to the total weight of the solution. The growth followed the step-flow mechanism. The step height is between 7 and 10 Å, which corresponds to 1-1.5 unit cells. The average step width is 200 nm. In contrast to Fig. 2a, no hint for possible impurity trapping can be found.

Growth Velocity

Layers grown according to the step-flow mechanism were cut perpendicular to (001) and (010) faces and the thicknesses were measured under a microscope. The results give the average growth velocities, $\bar{V}$, which take into account a possible dissolution process at the early stage of the growth experiment. The results obtained for $BaS_{1-x}Mn_xO_4$ with $0 \leq x \leq 0.003$ are $\bar{V}_{\langle 001 \rangle} = 7.8$ Å s^{-1} and $\bar{V}_{\langle 010 \rangle} = 10.3$ Å s^{-1}, which correponds to one and two unit cells per second, respectively. The growth time was longer than 100 h.

X-ray Powder Diffraction

Figures 3a-b show the XRD patterns of $BaSO_4$ and $BaS_{1-x}Mn_xO_4$, respectively, in terms of intensity versus 2-Θ. The baryte-II phase was confirmed in both cases. Other phases were not found in the solid-solution $BaS_{1-x}Mn_xO_4$ layers. A precise estimation of the lattice parameters of $BaSO_4$ (Fig. 3a) was made, resulting in $a_0 = 8.8854$ Å, $b_0 = 5.4558$ Å, and $c_0 = 7.1585$ Å. These values are in good agreement with those reported in the literature [9]. Figure 3b shows the XRD measurement of the $BaS_{0.999}Mn_{0.001}O_4$ powder. The lattice parameters are $a_0 = 8.8852$ Å, $b_0 = 5.4547$ Å, and $c_0 = 7.1591$ Å. The FWHM value estimated using the (002) reflex of a
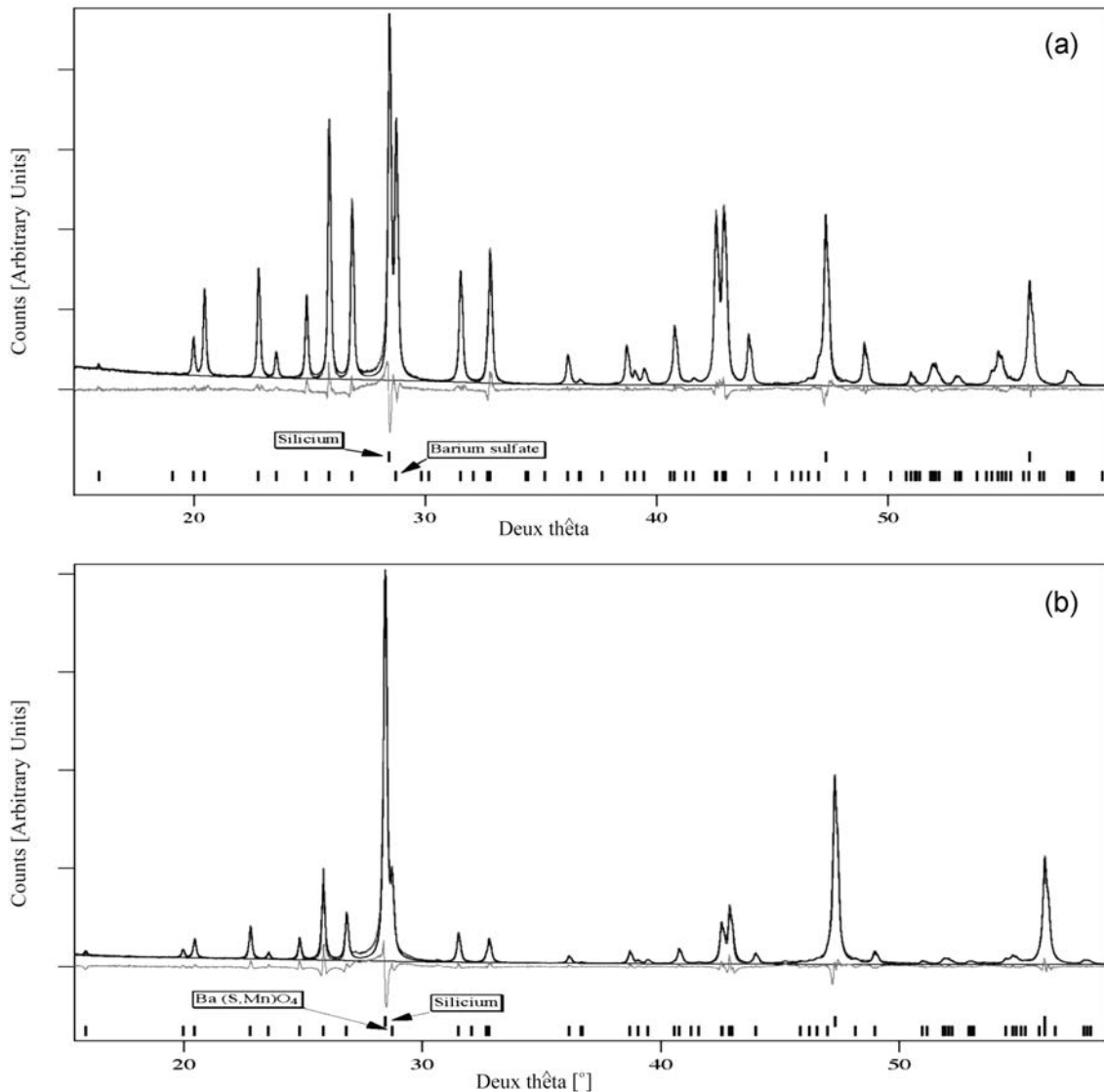
Fig. 3. XRD measurements of (a) $BaSO_4$ and (b) $BaS_{0.999}Mn_{0.001}O_4$.

single crystal of $BaS_{0.999}Mn_{0.001}O_4$ of 3 mm in size was measured to be $\Theta = 0.25°$.

Defect density

The epd was analyzed for $BaS_{0.999}Mn_{0.001}O_4$ films grown on LPE-grown $BaSO_4$ substrates. The etchant was the eutectic composition of NaCl-KCl-CsCl. For (011) faces, we found an epd of 1×10^3 to 4×10^4 cm^{-2}, thus the average spacing is between 300 and 50 μm. For (001) faces, an epd of 7×10^4 to 4×10^5 cm^{-2} was found, thus the average spacing is between 40 and 16 μm. I.e., less crystal defects pass through the (011) surface than through the (001) surface. In flux-grown samples, we counted between 3×10^4 and 2×10^5 etch pits (ep) cm^{-2} for (011) surfaces and about 2×10^6 ep cm^{-2} for (001) faces. Thus, by following our concept for the growth of high-quality $BaS_{1-x}Mn_xO_4$ layers, the epd for (011) and (001) faces could be reduced in average by about one order of magnitude.

Stability and Incorporation of Mn^{6+}

The liquid solution appears in an emerald color when containing Mn^{6+} ions. The color of Mn^{6+}-doped $BaSO_4$ crystals ranges from pink for small Mn^{6+} concentrations to violet for Mn^{6+} concentrations > 200 ppm wt. Two parameters, the stability of Mn^{6+} in the solution and the incorporation of Mn^{6+} into the $BaSO_4$ crystal, govern the Mn^{6+} concentration $c_{Mn^{6+}}$ in the crystal, resulting in striking differences between the initial $c_{Mn^{6+}}$ in the solution and the $c_{Mn^{6+}}$ detected in the grown layers. The reduction of Mn^{6+} in the solution MnO_2 and the formation of solid and its precipitation as dark brown clusters at the bottom of the crucible decreases $c_{Mn^{6+}}$ during the growth process. This makes the calculation of the segregation coefficient k_0 impossible. The reduction process starts immediately after the solid-to-liquid phase transition of the solution during heating up and continues with progressing growth duration until
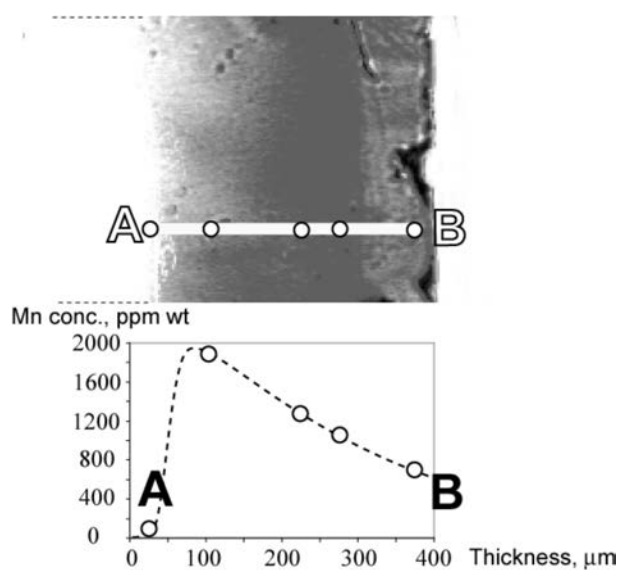
Fig. 4. Cross-section of a Mn^{6+}-doped crystal (top) and the Mn^{6+} concentration measured by EPMA.

the liquid solution becomes colorless. The time dependence of $c_{Mn^{6+}}$ in the solution was studied in [3]. The findings indicate that short-term experiments would be preferable but will result in thin layers only.

Results obtained by luminescence emission spectroscopy [1, 2, 10] suggest that the Mn ions are incorporated into the crystal predominantly as Mn^{6+}. Figure 4 shows the EPMA study of the Mn concentration in a cross-section of a BaSO$_4$ crystal. The growth proceeded in the direction from A to B. The $c_{Mn^{6+}}$ measured in different regions of the crystal is shown in the graph. The first measured point is in the undoped region of the crystal. As can be seen, $c_{Mn^{6+}}$ decreases by more than a factor of two from 2100 ppm to 800 ppm during the growth process. When investigating several samples, differences between the initial $c_{Mn^{6+}}$ in the solution and the $c_{Mn^{6+}}$ detected in the sample were up to one order of magnitude. As a consequence, the incorporation of Mn^{6+} into the host crystal BaSO$_4$ cannot be controlled precisely.

Summary

In this paper, we have discussed our work on the Mn^{6+}-doping of BaSO$_4$. Applying an advanced growth strategy, high-quality layers of BaS$_{1-x}$Mn$_x$O$_4$ have been grown by LPE. The problem of reproducible Mn^{6+} doping due to the reduction of Mn^{6+} is recognized. Mn^{6+} can be incorporated into BaSO$_4$ in quantities smaller than the initial manganese concentration.

Acknowledgements

References

1. T.C. Brunold and H.U. Güdel, Inorg. Chem. 36 (1997) 1946-1959.
2. D. Ehrentraut, M. Pollnau, and S. Kück, Appl. Phys. B75 (2002) 59-62.
3. Y.E. Romanyuk, D. Ehrentraut, M. Pollnau, S. García-Revilla, and R. Valiente, "Low-temperature flux growth of sulfates, molybdates, and tungstates of Ca, Sr, and Ba and investigation of doping with Mn^{6+}", Appl. Phys. A79, online version available (2004) 613-618.
4. D. Ehrentraut, Ph.D. thesis, Swiss Federal Institute of Technology, Lausanne, 2003.
5. D. Ehrentraut and M. Pollnau, J. Cryst. Growth 234 (2002) 533-538.
6. R.A. Young, ed., *The Rietveld Method*, IUCr Monographs on Crystallography No. 5 Published for the International Union for Crystallography by Oxford University Press, Oxford, UK, 1993.
7. A.B. Chase, in: *Preparation and Properties of Solid State Materials*, ed. R.A. Lefever, Dekker, New York, 1971.
8. A.A. Chernov, *Modern Crystallography III: Crystal Growth*, Springer Series in Solid-State Sciences 36, Springer-Verlag, Berlin, Heidelberg, New York, Tokyo, 1984.
9. Landoldt-Börnstein, *Zahlenwerte und Funktionen aus Naturwissenschaften und Technik*, Neue Serie, Gesamtherausgabe: K.-H. Hellwege, Bd. 7, *Kristallstrukturdaten anorganischer Verbindungen*, W. Pies, A. Weiss, Teil f, Springer, Berlin, Heidelberg, New York, 1977.
10. T.C. Brunold, H.U. Güdel, S. Kück, G. Huber, J. Opt. Soc. Am. B14 (1997) 2373-2378.